CHIN. PHYS. LETT. Vol. 37, No. 7 (2020) 070701

A New Approach for Residual Stress Analysis of GH3535 Alloy by Using Two-Dimensional Synchrotron X-Ray Diffraction

Sheng Jiang(蒋升)[1,2*], Ji-Chao Zhang(张继超)[1], Shuai Yan(闫帅)[1], and Xiao-Li Li(李晓丽)[2]

[1]*Shanghai Advanced Research Institute, Chinese Academy of Sciences, Shanghai 201210, China*
[2]*Shanghai Institute of Applied Physics, Chinese Academy of Sciences, Shanghai 201203, China*

(Received 31 December 2019; accepted 9 May 2020; published online 21 June 2020)

We propose a new method to evaluate residual stress based on the analysis of a portion of a Debye ring with two-dimensional synchrotron x-ray diffraction. The residual stress of a nickel-based alloy GH3535 evaluated by the proposed method is determined to be -1149 ± 34 MPa based on the quantitative analysis of the deformation of the (200) reflection, and the residual stress obtained by analyzing THE (111) plane is -933 ± 68 MPa. The results demonstrate that the GH3535 alloy surface is highly compressive, as expected for a polishing surface treatment. The proposed method provides insight into the field of residual stress measurement and quantitative understanding of the residual stress states in GH3535.

PACS: 07.85.Qe, 68.35.Gy, 61.66.Dk, 61.72.Dd DOI: 10.1088/0256-307X/37/7/070701

A nickel-based alloy GH3535 has been developed and identified as the primary structural material in the thorium molten salt reactor because of its excellent corrosion resistance and mechanical performance.[1−4] The existence of residual stresses has a significant impact on its performance, with impacts such as crack failure, fatigue strength, stress corrosion and shape accuracy.[5] It is therefore crucial to evaluate the microstructure of and residual stress in this alloy.

Non-destructive x-ray diffraction (XRD) stress measurement is an effective tool for determining residual stress.[6−11] The conventional x-ray stress measurement with laboratorial sources and a point or line detector is called the $\sin^2\psi$ method, where ψ represents the angle between the sample surface normal (S_z) and scattering vector ($\boldsymbol{q}$), as shown in Fig. 1.

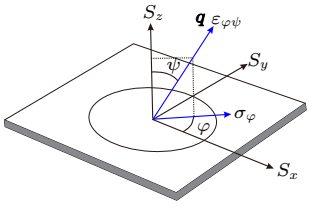

Fig. 1. Definition of sample coordinate systems (S_x, S_y, S_z) for strain $\varepsilon_{\phi\psi}$ and stress σ_ϕ. The stress measurement direction is along diffraction vector $\boldsymbol{q}$.

Recently, two-dimensional (2D) detectors have been readily available for laboratory x-ray diffractometers.[12,13] Gelfi *et al.* analyzed a Debye ring with the stress measurement (DRAST) method.[14−16] In addition, Tanaka *et al.* proposed the $\cos\alpha$ method for determination of the stress state.[17−19] It was confirmed that both DRAST and the $\cos\alpha$ method provide stress values consistent with the $\sin^2\psi$ method.[14,20,21] However, conventional x-ray sources have limitations in terms of spatial resolution and data collection time.

Over the past decade, with the high flux and brightness of the 3rd generation synchrotron radiation facility, synchrotron x-ray diffraction (SXRD) has become a powerful tool for studying surfaces, multilayers or microstructures with high spatial resolution.[22−27] It is expected that SXRD in combination with 2D detectors would be effective for quick and accurate stress analysis. While the majority of stress measurements using SXRD are currently based on the conventional $\sin^2\psi$ methods, in comparison, the 2D x-ray stress approach usually employs the x-ray tube as the x-ray source, such as the $\cos\alpha$ method,[17,18] which employs an area detector placed in the back scattering configuration to record the whole backward diffraction ring ($2\theta > 90°$).

In this letter, we present a new residual stress determination method based on 2D synchrotron x-ray micro-diffraction. It can be used to measure the stress by analyzing only a portion of a single forward diffraction ring ($2\theta < 90°$) without the sample rotation during the whole process. The residual stress of GH3535 is evaluated, and the results demonstrate that the GH3535 alloy surface is highly compressive.

The 2D SXRD measurements were performed with the BL15U1 beamline at the Shanghai Synchrotron Radiation Facility (SSRF),[28] at a wavelength of 0.7293 Å. XRD patterns were recorded by an MAR-CCD 165 area detector. The experiment geometry is accurately determined by calibrating CeO_2 standard samples. The beam spot is approximately 5(horizontal) × 3(vertical) μm^2.

The chemical compositions (in wt%) of the GH3535 used in the present study are listed in Table 1. Figure 2 displays the surface morphology of

Supported by the National Key Scientific Instrument and Equipment Development Projects of China under Grant No. 2017YFA0403401, the Natural Science Foundation of Shanghai under Grant No. 18ZR1448100, and the National Natural Science Foundation of China under Grant Nos. 11705270 and 11104307.
*Corresponding author. Email: jiangsheng@sinap.ac.cn
© 2020 Chinese Physical Society and IOP Publishing Ltd

this material, which consists of the equi-axed grains with an average size of 60 μm.

Table 1. Chemical composition of the experimental alloy in units of wt%.

Mo	Cr	Fe	Mn	Si	C
16.7	7.07	4.19	0.67	0.46	0.012
Co	Cu	P	S	Ni	
0.009	0.006	0.005	0.001	Balance	

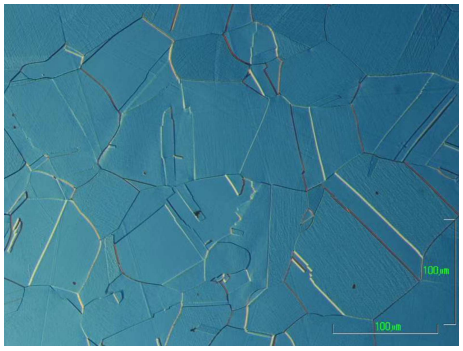

Fig. 2. Microstructure of the GH3535 alloy observed by optical metallography.

Residual stress is usually expressed in terms of the strain components in sample coordinates. Nevertheless, the diffraction vector $\boldsymbol{q}$ which defines the normal direction of the diffraction plane is defined with respect to the laboratory coordinate system by 2θ and γ, where θ is the diffraction angle and γ is the rotation angle on the diffraction cone, as shown in Fig. 3(a).

To demonstrate the relationship between residual stress and XRD measurements, it is necessary to build two coordinate systems, the laboratory (diffractometer) coordinate system (L_x, L_y, L_z) and the sample coordinate system (S_x, S_y, S_z) [Fig. 3(a)]. The geometric definition of the sample during the stress measurements is displayed in Fig. 3(c).

In the laboratory coordinate system, L_y and L_z are fixed on the Debye ring plane, L_x is defined by the incidence beam direction, L_y is defined in vertical direction, and L_z is chosen to form the right hand spiral coordinate system with L_x and L_y.

In the sample coordinate system (S_x, S_y, S_z), S_x and S_y are always associated with the sample surface, and S_z is that of the surface normal.

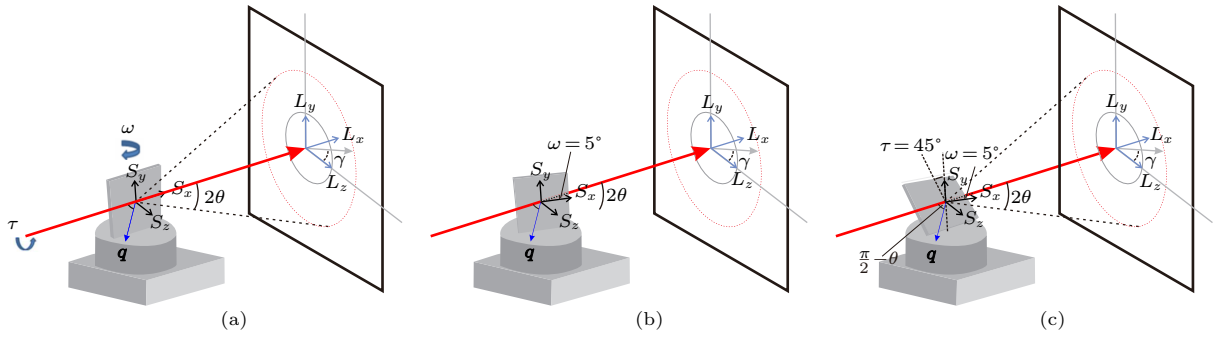

Fig. 3. Geometric definition of the sample reference system (S_x, S_y, S_z) and laboratory coordinates (L_x, L_y, L_z): (a) sample reference system (S_x, S_y, S_z) and laboratory coordinates (L_x, L_y, L_z), (b) clockwise ω around the L_y axis, (c) clockwise τ around the L_x axis.

The unit vector of a diffraction vector q_L in the laboratory system is given as

$$q_L = \begin{pmatrix} -\sin\theta \\ \cos\theta\sin\gamma \\ \cos\theta\cos\gamma \end{pmatrix}, \tag{1}$$

where the vector q_L describes a diffraction cone when γ takes values from 0 to 360° [Fig. 3(a)].

To determine the transformation matrix that relates the coordinates q_L [Fig. 3(a)] in the laboratory system to $\boldsymbol{q}_S$ [Fig. 3(c)] in the sample system, we consider two step sample rotations (ω, τ) defined in Figs. 3(b) and 3(c).

First, the (L_x, L_y, L_z) system rotates clockwise ω angle around the L_y axis, as shown in Fig. 3(b). The corresponding rotational matrix is

$$R(L_y) = \begin{pmatrix} \cos\omega & 0 & \sin\omega \\ 0 & 1 & 0 \\ -\sin\omega & 0 & \cos\omega \end{pmatrix}. \tag{2}$$

Second, for the clockwise rotation around the L_x axis with the angle τ [Fig. 3(c)], the rotational matrix is

$$R(L_x) = \begin{pmatrix} 1 & 0 & 0 \\ 0 & \cos\tau & -\sin\tau \\ 0 & \sin\tau & \cos\tau \end{pmatrix}. \tag{3}$$

Accordingly, the resulting transformation matrix R is

$$\begin{aligned} R &= R(L_x)\cdot R(L_y) \\ &= \begin{pmatrix} \cos\omega & 0 & \sin\omega \\ \sin\tau\sin\omega & \cos\tau & -\sin\tau\cos\omega \\ -\cos\tau\sin\omega & \sin\tau & \cos\tau\cos\omega \end{pmatrix}. \end{aligned} \tag{4}$$

Therefore, the unit vector $\boldsymbol{q}_S$ of the diffraction vector in the sample coordinates (S_x, S_y, S_z) is given by

$$\boldsymbol{q}_S = R\cdot\boldsymbol{q}_L = \begin{pmatrix} \kappa_{11} \\ \kappa_{12} \\ \kappa_{13} \end{pmatrix}. \tag{5}$$

$$\begin{aligned}\kappa_{11} &= -\cos\omega\sin\theta + \sin\omega\cos\theta\cos\gamma,\\ \kappa_{12} &= \sin\tau\sin\omega\sin\theta + \cos\tau\cos\theta\sin\gamma\\ &\quad -\sin\tau\cos\omega\cos\theta\cos\gamma,\\ \kappa_{13} &= \cos\tau\sin\omega\sin\theta + \sin\tau\cos\theta\sin\gamma\\ &\quad +\cos\tau\cos\omega\cos\theta\cos\gamma.\end{aligned}$$

On the other hand, the scattering vector $\boldsymbol{q}_S$ is also defined as

$$\boldsymbol{q}_S = \begin{pmatrix}\sin\psi\cos\phi\\ \sin\psi\sin\phi\\ \cos\psi\end{pmatrix}. \tag{6}$$

On the bases of Eqs. (5) and (6), the angles ϕ and ψ are given by

$$\begin{aligned}\cos\psi &= \cos\tau\sin\omega\sin\theta + \sin\tau\cos\theta\sin\gamma\\ &\quad +\cos\tau\cos\omega\cos\theta\cos\gamma, \qquad (7)\\ \cos\phi &= (-\cos\omega\sin\theta + \sin\omega\cos\theta\cos\gamma)/\sin\psi. \qquad (8)\end{aligned}$$

For each point (θ, γ) of the Debye ring, the corresponding (ϕ, ψ) values are determined. As the x-ray penetrates a few micrometers from the metal surface, the measured stress value can be assumed to be the value under planar stress. Based on elastic theory, the stress can be expressed as

$$\sigma_\phi = \frac{1}{d_0}\frac{E}{1+\nu}\frac{\partial d_{\phi\psi}}{\partial \sin^2\psi}, \tag{9}$$

where $d_{\phi\psi}$ is the lattice spacing of the sample and d_0 is the lattice spacing in the stress-free state. E is the Young's modulus, and ν is Poisson's ratio. With the (ϕ, ψ) value obtained from Eqs. (7) and (8), the stress σ_ϕ can be determined from the slope in the relation between $d_{\phi\psi}$ and $\sin^2\psi$ based on Eq. (9).

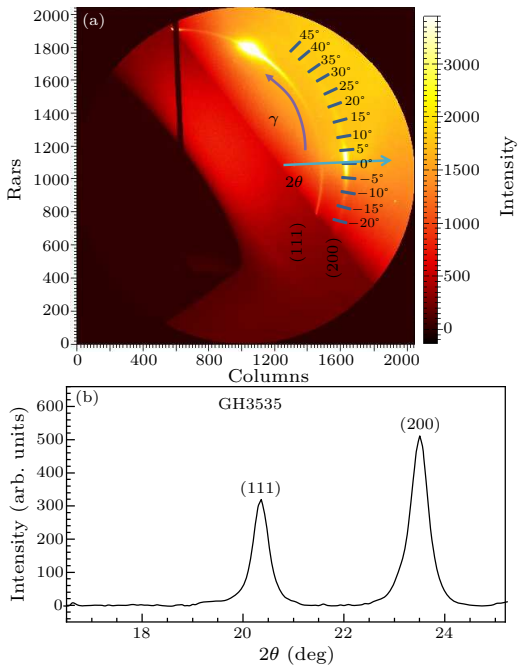

Fig. 4. (a) Typical 2D XRD patterns and (b) integrated 1D XRD patterns of GH3535.

Typical 2D Debye rings of a GH3535 alloy are displayed in Fig. 4(a). Two rings of the (111) and (200) planes are evident in the XRD image. First, the quantitative analysis of the deformation of the (200) reflection is selected to perform the residual stress measurement. To determine the 2θ value corresponding to a certain γ angle, the integration range from $-20°$ to $45°$ with a step of $\Delta\gamma = 5°$ is performed on the XRD image. The diffraction profile at each γ value is integration in the range $\gamma - \frac{1}{2}\Delta\gamma$ to $\gamma + \frac{1}{2}\Delta\gamma$.

The collected images were integrated into one-dimensional (1D) diffraction patterns by the software FIT2D.[29] The typical integrated 1D XRD patterns are shown in Fig. 4(b).

For stress calculation, the Young's modulus (E) of 168 GPa and Poisson's ratio (ν) of 0.35 for the (200) reflection were adopted.[30] Taking $\tau = 45°$, $\omega = 5°$, the d–$\sin^2\psi$ plot of the (200) reflection and its linear fit are shown in Fig. 5. It is clear that they have linear relation, confirming the biaxial stress state for this alloy; the simulations give the fitting slope values of -0.0166 ± 0.0005, and the value of d_0 (1.798 Å) is equal to the data found for $\psi = 0$. According to Eq. (8), the residual stress of $\sigma_\phi = -1149 \pm 34$ MPa is determined. Herein, the negative values of σ_ϕ represent a compressive stress state. The measurement indicates that the residual stress in the GH3535 alloy surface is highly compressive, as expected for a polishing surface treatment.

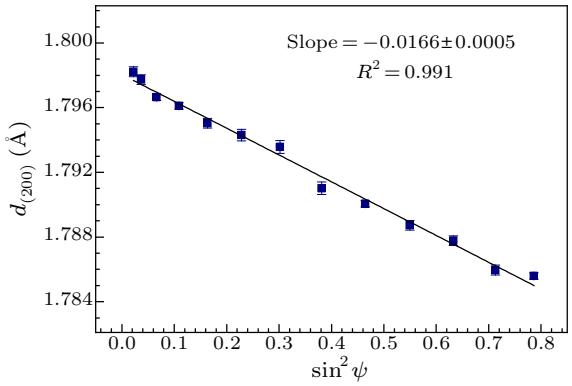

Fig. 5. Plotting and linear fitting of the values of d-spacing of (200) plotted against $\sin^2\psi$ for GH3535.

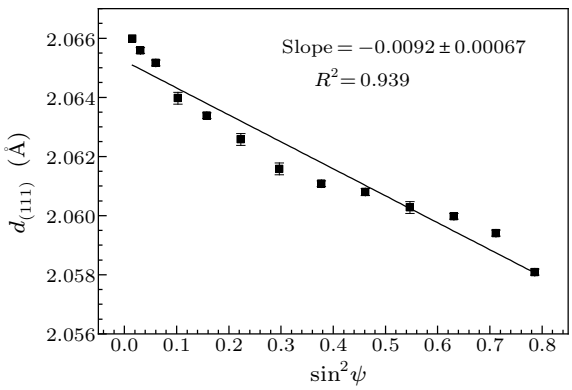

Fig. 6. Plotting and linear fitting of d–$\sin^2\psi$ diagrams obtained for GH3535, calculated for the (111) planes.

To compare the stress between different crystal

planes, the residual stress was also calculated from the analysis of the (111) plane. The d–$\sin^2\psi$ plot of the (111) is shown in Fig. 6. The linear fitting gives slope values of -0.0092 ± 0.00067. Taking the advantage of the Young's modulus of 264 GPa and Poisson's ratio of 0.26 for (111) plane, the calculated stress from the linear fitting is determined to be -933 ± 68 MPa, which is somewhat lower than that of the value obtained by the (200) plane.

Moreover, to verify this new 2D method, the stress value is compared with that obtained by the conventional $\sin^2\psi$ method. When $\gamma = 0°$ and $\tau = 0°$, the geometric definition is a typical setup for a diffractometer, and the 2D method is simplified to the conventional $\sin^2\psi$ method. Then a total of five frames taken with five different ω angles (at 2°, 5°, 10°, 20° and 30°) are used to calculate residual stress with the conventional $\sin^2\psi$ method. The frame collected at $\omega = 5°$, as an example, is shown in Fig. 7. The d–$\sin^2\psi$ fitting on the (200) peak gives a residual stress of -1089 ± 129 MPa, which is at the same level as that of the value obtained by the new 2D method. However, the 2D method gives some lower statistical errors because of the increasing number of data points.

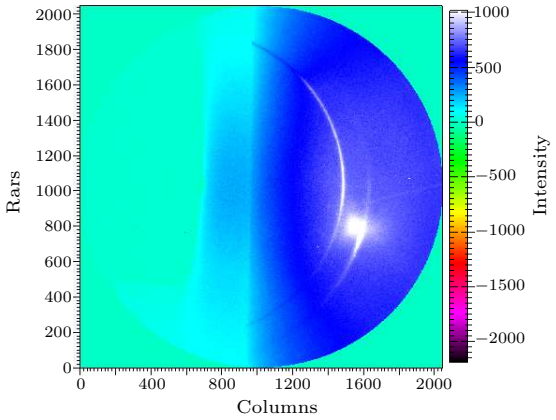

Fig. 7. Two-dimensional XRD patterns of GH3535 obtained at $\omega = 5°$ and $\tau = 0°$.

In conclusion, we have proposed a new method based on the analysis of a portion of a Debye ring for evaluating the residual stress of a GH3535 alloy. The residual stress is determined to be -1149 ± 34 MPa, based on the analysis of the deformation of the (200) reflection, which demonstrates that the GH3535 alloy surface is highly compressive due to the polishing treatment of the surface.

References

[1] Jiang M H, Xu H J and Dai Z M 2012 *Bull. Chin. Acad. Sci.* **27** 366 (in Chinese)
[2] Gao J, Huang H F, Liu J H *et al.* 2018 *Appl. Phys.* **123** 205901
[3] Gao J, Huang H F, Liu Z J *et al.* 2019 *J. Appl. Phys.* **125** 055901
[4] Liu T, Dong J S, Wang L *et al.* 2015 *J. Mater. Sci. & Technol.* **31** 269
[5] Yu K, Jiang Z G, Leng B *et al.* 2016 *Opt. Laser Technol.* **81** 18
[6] Shi Y, Zheng C, Ren M Q *et al.* 2017 *Polymer* **123** 137
[7] Wei Y, Cheng H B, Wang X Y *et al.* 2012 *Appl. Phys. Lett.* **101** 231909
[8] Badawi K F, Villain P, Goudeau P *et al.* 2002 *Appl. Phys. Lett.* **80** 4705
[9] Welzel U, Kumar A and Mittemeijer E J 2009 *Appl. Phys. Lett.* **95** 111907
[10] Kurz S J B, Welzel U, Bischoff E *et al.* 2014 *J. Appl. Crystallogr.* **47** 291
[11] Zhang J M and Xu K W 2005 *Chin. Phys.* **14** 1866
[12] Tanaka K 2018 *J. Appl. Crystallogr.* **51** 1329
[13] Zhang Z W, Feng Y F, Tan Q *et al.* 2019 *Mater. & Des.* **166** 107603
[14] Gelfi M, Vecchia G M L, Lecis N *et al.* 2005 *Surf. Coat. Technol.* **192** 263
[15] Gelfi M, Bontempi E, Roberti R *et al.* 2004 *Acta Mater.* **52** 583
[16] Gelfi M, Bontempi E, Roberti R *et al.* 2004 *Thin Solid Films* **450** 143
[17] Sasaki T, Takahashi S, Iwfuchi K *et al.* 2006 *Mater. Sci. Forum* **524** 381
[18] Sasaki T, Koda K, Fujimoto Y *et al.* 2014 *Adv. Mater. Res.* **922** 167
[19] Sasaki T, Maruyama Y, Ohba H *et al.* 2014 *J. Instrum.* **9** C07006
[20] Shabadi R, Ionescu M, Jeandin *et al.* 2018 *Mater. Sci. Forum* **941** 2407
[21] Zhu P F, Gou G Q, Li Z F *et al.* 2019 *Int. J. Mod. Phys. B* **33** 1940032
[22] Mitsui S, Sasaki T, Arai Y *et al.* 2019 *Nucl. Instrum. Methods Phys. Res. Sect. A* **924** 441
[23] Sasaki T, Ishikawa F and Takahasi M 2016 *Appl. Phys. Lett.* **108** 012102
[24] Hammer R, Todt J, Keckes J *et al.* 2017 *Mater. & Des.* **132** 72
[25] Connolly M, Park J S, Bradley P *et al.* 2018 *Rev. Sci. Instrum.* **89** 063701
[26] Izumi A, Kakara T, Otsuki M W *et al.* 2019 *Polymer* **182** 121857
[27] Jiang L, Ye X X, Wang D J *et al.* 2020 *Nucl. Sci. Tech.* **31** 6
[28] Zhang L L, Yan S, Jiang S *et al.* 2015 *Nucl. Sci. Tech.* **26** 060101
[29] Hammersley A P, Svensson S O, Hanfland M *et al.* 1996 *High Press. Res.* **14** 235
[30] Eigenmann B and Macherauch E 1996 *Mater. Sci. Eng. Technol.* **27** 426